Al-Azhar Bulletin of Science, Section D, Vol. 33, No. 1 (June) 2022, pp. 163-177
http://doi. 10.21608/absb.2022.98110.1140

Al-Azhar Bulletin of Science: Section D

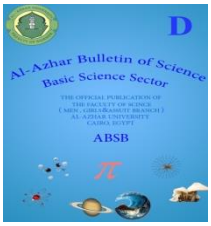

APPLICATION OF SEDIMENTOLOGICAL AND RADIOMETRIC STUDIES TO EVALUATE THE SUBSURFACE SOIL FOR SOME LOCALITIES OF NEW ADMINISTRATIVE CAPITAL AREA OF EGYPT.

Ibrahim H. Othman [a,] *, Ahmed M. Saad [b], Osama M. Draz [c].

[a] National Egyptian Drilling and Petroleum Services, Al-Mokattem, Cairo, Egypt.
[b] Geology Department, Faculty of Science (Boys), Al-Azhar University, Cairo, Egypt.
[c] Exploration Department, Nuclear Material Authority, Al-Kattamia, Cairo, Egypt.
* Corresponding Author: ibrahimhamdi38@gmail.com
Received: 27 Sep 2021; Revised: 10 Jan 2022; Accepted: 10 Jan 2022; Published: 01 Jun 2022

ABSTRACT

This article includes geological, sedimentological and radiometric studies on some localities of new Administrative Capital. The subsurface soil of the study area composed fundamentally of weathered doleritic basaltic rocks and gravely sand. The sedimentological study includes particle size distribution, X-ray diffraction (X R D) for detection of clay minerals and petrographical studies, to describe and evaluate the textural parameters and statistical measurements to recognize the depositional pattern of sediment samples in the study area. The textural parameters results are graphic mean size varying from (-1.499ϕ) to (5.195ϕ) where the average is (1.205ϕ) indicating medium sand grained. The sorting (σI) ranges from (0.307ϕ) to (3.255ϕ) with an average (2.297ϕ) falling in very poorly sorted. The skewness (SkI) ranges from (-0.323ϕ) to (0.838ϕ) with an average of (0.361ϕ) reflecting strongly fine-skewed. The kurtosis (KG) oscillates from (0.699ϕ) to (4.348ϕ) with an average (1.26ϕ) proving Leptokurtic. Through the study of different relations between the grain size parameters, it was clear that deposition environment of the study area sediment samples is a river environment. The identification of the clay minerals using X-ray diffraction analysis involved that the clay minerals are montmorillonite and kaolinite. Petrographically, the studied samples clear that the basaltic rocks are classified as doleritic olivine basalts and the non-carbonate microfacies are classified as quartz arenite type. Siliceous and calcareous cement is commonly cement in sandstone samples. The results of radiometric examining confirm that the soil is unharmed to human activities where all radionuclides concentration ^{232}Th, ^{238}U, ^{226}Ra, ^{40}K and radium equivalent (Ra_{eq}) ranged from 1.24 to 13.59; 8.12 to 20.3; 22.2 to 55.5; 71.99 to 369.34, from 47.09 to 108.87 with average values 7.09, 15.41, 39.56, 249.12, 80.78 Bqkg^{-1} respectively and lower than (370 Bq/kg), external hazard index (H_{ex}) range from 0.13 to 0.29 Bqkg^{-1} with an average 0.218 which is lower than (1 Bq/kg) and effective dose rate (D_{eff}) range from 26.78 to 62.94 with a mean average value 46.79 μSvyr^{-1} as far below (70 μSv y^{-1}) all radioactive measurements are lower than recommendable by **(IAEA).**

Keywords: Textural parameters; X-ray diffraction; Clay minerals; Petrography; Radiometric.

1. INTRODUCTION

A good and wise way to solve the problems of over crowdedness in Cairo and busy areas is to build new cities and reconstruct our desert. The approximate area of the New Administrative Capital is 700 Km^2 and located in eastern Cairo. It stretches between the Nile River and the Suez Canal, thus, having strategic location the eastern part of Cairo and has a good climate. It is expected that it will accommodate 6.5 million people in 20 residential areas and include a road network that are length to 650 Km, international airport and involve the longest tower in the continent which is Iconic

Tower. Some localities of New Administrative Capital (the study area) include the fifth residential neighborhood -R5- which is the second area in the residential neighborhood named New Garden City. About 714 residential buildings are being implemented, and it is planned to include more than 24000 housing units. The study area also includes the University of Hertfordshire (UH) as the first full branch of a British University in Egypt, the Tiba Rose Hotel (Air Defense House) and electrical generation station. The study area suffers from some problems, such as existence of clay layers which resemble one of the most important problems in several beds, which causes a significant risk to urbanization. Water content changes leads to volume change of clayey soils; also moisture content controls expansive clay characteristics such as shrinking and swelling properties which lead to damage to constructions **[1,2].** Also, several problems facing civil buildings that are built over this soil due to its high settlement, permeability and has low values of shear quality **[3,4]**. Soil stabilization is commonly used to increase durability and strength and reduce plastic index or swelling potential by adding chemical additives and wastes of industries as; bottom, fly ash and lime **[5-12].** Different studies have been achieved in this area and the regions of Cairo Suez District as a whole. These studies involve geology, sedimentology, geomorphology, structures and engineering geology (e.g. **[13- 21]**).

Hagag [22] concluded that the entire Cairo Suez District and Gebel Um Reheiat - Gebel Qattamiya area, in the north Eastern Desert of Egypt are highly deformed by continental rifting. Structures of Rift-related are dominantly distinguished by E to NW, NNW and WNW oriented faults. Radiometric studies have also been done on several samples of study area. One of natural risk and hazard phenomenon is called radioactivity, it can lead to loss of life, damage, disturbance of social life and economy. When occur large increasing of radioactivity of a particular rock over its background more than twice is called anomaly. The aim of this research is collecting data about the subsurface soil to evaluate it for engineering purposes using sedimentological and radiometric studies.

2. Location and geologic setting:

The New Administrative Capital City lies at the east of Cairo-Suez road and west of new ring road. The study area is located between longitudes 31° 37′ 29"- 31° 39′ 46" E and latitudes 29° 59′ 31"- 30° 0′ 28" N. (Fig. 1). **[23]** Classified the Cairo-Suez Desert road into the following geomorphic units: Mokattam-Ataqa upland, Cairo-Suez foot hills, Drainage pattern, Sand dunes, Low land area. The cropping out of Gebel Shabrweet core are the Cretaceous strata and oldest exposed rocks in the Cairo-Suez road, which are include two main rock units, **[24].** The Fayid Formation is lower unit about 12 meters thick is fundamentally composed of shales and marl. The upper unit is Galala Formation composed of limestones having about 269 m thick. The Eocene successions unconformably rest on the Upper Cretaceous beds, unconformabley overlying the Upper Eocene beds. The Oligocene sequence is divided into loose sand and gravels at the base and basaltic flows at the top. A note worthily thickness increasing of the Oligocene sediments is shown on going from east to west, whereas the Miocene sediments unconformably overlie the Oligocene rocks in many areas.

The Miocene sequence is classified into two units; the marine Miocene sediments at the base and the non-marine Miocene sediments at the top. The two units are separated by an unconformity surface. The marine Miocene rocks consist mainly of limestones, shales and sandstones; they get more calcareous both temporally and eastward. The non-marine Miocene rocks are mainly made up of gravels, sandstones, clays and few limestones being distinct from the Oligocene sediments by their light color and finger grains size. (Fig.2)

Structurally, the structural setting of New Administrative Capital City belongs to that of the central part of Cairo Suez District. The study area is marked by three structure types; are

faults, fractures, unconformity and folds. The regional dip is gentle of the Miocene strata, except monoclines may up to 27° and faults neighborhood. The most predominant structure in New Administrative Capital City is faulting. The whole faults distinguished are normal fault plane and steeply dipping. The faults have two major trends; the NW-SE, and the E–W Mediterranean. The direction alteration of NW–SE faults lead to bend into direction of E–W. Majority of the folds are rather small flexures relative and parallel to the faults neighboring them. There are too minor monoclinal wrinkles, which are formed by the stretching of the beds before their factual rupture by faulting. Minor and major unconformities are general in the region. The major is that between the Cretaceous and Eocene formations. A small numbers of minor unconformities are demonstrated in the area. (Fig.3)

3. MATERIALS AND METHODS:

3.1 Collection of samples:

A total of fifty-two samples collected from 44 bore hole representative sedimentary samples from the different localities in The New Administrative Capital City by rotary mechanical rig at depths from zero to 15 meters (from the surface of the ground) for laboratory analysis (Fig. 1).

3.2 Sedimentological studies:

Three main parts of the sedimentological studies involve; particle size distribution of sand, X-ray diffraction analysis (X R D) for clay minerals and the petrographical studies to obtain information related to the depositional environments. The different sedimentary facies forming the sedimentary succession and their mutual relationships are to be emphasized. The depositional interpretations will be given to infer the evolution of these sediments.

3.2.1 particle size analysis:

The results of particle size measurements is most important to detect sediments behavior during transportation and deposition. It is also used to determine description, textural and to evaluate the subsurface sediments, each sample was sieved at half phi intervals down to (5ϕ) sieve **[25].** Thus, the sediments were analyzed using Gradistat software version 8.0 **[26]** with the grain size classification of **[27].** The parameters calculated were kurtosis (KG), sorting (σI), the mean (Mz) and skewness (SkI). There are many attempts by making relationships between different calculated parameters from particle size distribution of sands to several depositional processes and environments. **[28]** Suggested that the plot of standard deviation (σI) against median size. (Fig. 6) provides best way for differentiating between river, quiet water, wave processes and inner shelf. The most of the studied samples were existed to be related to inner shelf. On the other hand **[29]** mentioned that it is possible to differentiate between dune, river and beach environments. **[30]** Deduced that a plot between skewness and standard deviation is further effective in distinguishing beach and river sands. By applying this relationship for investigated sediments (Fig.7), all the samples fall in river field. **[31]** Used the textural parameters derived by **[25]** in various combinations as environmental indications. They found that the plot diagram between (Mz) against (σI) is most effective in distinguishing between beach and river sands.

3.2.2 X-ray diffraction:

The clay minerals can only be detected by using X-ray diffraction and was achieved by using Philips X-R-D 9 type (PW 3711), with (Ni-filter) Cu Kα radiation. The studied samples were run from (2) to (50) ° 2 θ at (40) mA and (40) kV.

3.2.3 Methods of petrographical studies:

Some of the collected samples were studied petrographically using research polarizing microscope attached with camera (Nikon, United states) describe the microfacies associations of recognized non-marine Miocene and Oligo-Miocene rocks in the study area.

3.3 Radiometric measurements methods:

Thirty nine samples were collected from study area at different depths 2, 5, 10 and 15m. the samples taken from study area were tightly

closed after drying in a 100° oven and last for up to 4 weeks at least to reduce and limit the escape possible radon (> 7 half-live of ^{224}Ra and ^{222}Rn) before detection just because ensure that it's products of daughter as ^{226}Ra and ^{228}Th up to ^{210}Pb and ^{208}Pb respectively achieved secular balance by their respective radionuclide of parent. All measurements of soil samples in study area were implemented by spectrometer of (γ-ray) include (n-type) HPGe detector of coaxial type and its efficiency is 18%.

The concentration of radioactivity in the study area samples was gained by:

$$A\ (BqKg^{-1}) = C_n / \varepsilon_\gamma\ p_\gamma\ t\ m \quad \ldots \quad (1)$$

Whereas: (A), (C_n), (ε_γ), (P_γ), (m) and (t) are the activity concentrations, net count, absolute efficiency at energy of photo peaks, the emission of gamma ray, mass of the soil in (kg) and counting time in the second respectively.

The Radiological effects determined by subsequent equations:

a- Radium Equivalent Activity (Ra_{eq}) equation by **[32]** is:

$$Ra_{eq} = 1.43C_{Th} + C_{Ra} + 0.077C_k \quad \ldots \quad (2)$$

Whereas: C_{Th}, C_{Ra}, and $C_{k;}$ are factors of average activity concentration of soil and weathered doleritic basalt in study area in $Bqkg^{-1}$ of ^{232}Th, ^{226}Ra, and ^{40}K respectively.

b- Gamma absorbed dose rate (D_{rate}) equation by **[33]** is:

$$D_{rate} = 0.0414C_K + 0.461C_{Ra} + 0.623\ C_{Th} \quad \ldots \quad (3)$$

c- Effective dose rate equation by **[34]** is:

$$D_{eff} = 0.2 \times 8760\ h \times D \times 0.2 \times 0.7\mu Sv\ Gy^{-1} \times 10^{-3} \quad \ldots \quad (4)$$

d- External hazard index (H_{ex}) equation by **[35]** is:

$$H_{ex} = A_{Th}/259 + A_{Ra}/370 + A_K/4810 \leq 1 \quad \ldots \quad (5)$$

4 RESULTS AND DISCUSSION:

4.1 Sedimentological analysis:

4.1.1 Sieve analysis:

The particle size analysis results are displayed in table (1) and representing data using cumulative curves and histograms (Fig. 4 & 5). Histograms are built by plotting grade size and weight percent of particle size where histogram is the simplest type of graphical explanation. Histograms confirm that study area samples have a vast range of ϕ (phi) values of diameter which covering all medium to fine sand sizes. The constructed histogram indicate that the particle size of the studied samples is generally unimodal (20 samples) except 17 samples are bimodal and 4 samples show polymodal characteristics (Fig. 4).

Cumulative curve was designed by plotting the phi units against total weight percent of grain size (Fig. 5). The values of ϕ 5, ϕ 16, ϕ 25, ϕ 50, ϕ 75, ϕ 84, and ϕ 95 were determined by cumulative curves and the calculations of particle size parameters calculable according by the equation of **[25].** The table (1) shows parameters of particle size are, the graphic mean size, which varies from -1.499 ϕ to 5.195 ϕ with an average 1.205 ϕ and indicating medium sand grained. Skewness values from -0.323 ϕ strongly coarse-skewed to 0.838 ϕ strongly fine-skewed with an average 0.361 ϕ reflecting strongly fine-skewed. The sorting (σI) ranges from 0.307 ϕ very well-sorted to 3.255 ϕ very poorly-sorted with an average 2.297 ϕ falling in the very poorly sorted. The kurtosis ranges between 0.699 ϕ Platykurtic to 4.348 ϕ extremely leptokurtic with an average 1.26 ϕ proving Leptokurtic. Through the study of different relations between the grain size parameters, it was clear that deposition environment of the study area sediment samples is a river environment.

4.1.2 Mineralogical composition of clay:

The presence of clay minerals in soil increase their volume when existence of water. Dikite and kaolinite are nonexpansive minerals of clay and their values of water attracting index and plasticity index are low. But the expansive clay is montmorillonite mineral. The montmorillonite builds up of three layers including one of aluminum layer between two silicon layers. In some cases occur substitution parts of aluminum by iron or magnesium, and small quantities of calcium or sodium then attachment occurs, as ions existing inside the

three layers or nearby the crystal edges. Weak forces (Vander Waals) hold layers together and exchangeable ions have occurred. The swelling happen when water enter the montmorillonite bonds and causes separation of its layers. The most dominant clay minerals of some samples at study area is montmorillonite (Fig.9). The kaolinite, $Al_4Si_4O_{10}$ (OH) $_8$ is clay mineral consist of one alumina octahedral and one tetrahedral sheet mixed in units. The separation is difficult to happen between the sheets of kaolinite mineral as a result of hydrogen bond which hold its layers. The moist and warm environments is most commonly environment in which Kaolinite can be formed. The second diverse of clay samples is kaolinite mineral at study area (Fig.9). The diffraction analysis of X-ray confirms that samples of clay include of kaolinite and montmorillonite (Fig. 9) whereas montmorillonite has danger and harmful effect on construction and buildings as a result of swelling character higher than any clay minerals.

4.1.3 Petrography:

The International Society for Rock Mechanics **[36]** has published proposed methods for petrographically examining those rock properties that have an approach on mechanical behavior that can just be recognized with a microscope. The petrographical examining of study area which belongs to a new Administrative Capital indicates the presence of doleritic basaltic rocks and quartz arenite sandstone association. These are as follows:

4.1.3.1 Doleritic basaltic rocks:

Plagioclases, pyroxene, olivine are the main minerals constituents of the doleritic basalts and defined as fine to medium-grained and mainly magnetite as iron oxides. **Plagioclases** occur as crystals of subhedral prismatic texture about (220 µm), (300 µm) in width and length respectively and represented as a doleritic patterns. Plagioclases are overall fresh (Fig.10c). The **Pyroxene** (augite) angular crystals intersects between plagioclase crystals forming subophitic and ophitic like intergrowth textures (Fig.10d). And its color is Light green and brown. **Olivine** are in the form of large rounded subhedral to anhedral crystals, as a result of fast crystallization, olivine is the lower patterns in the rock, fine crystals of pyroxenes are considerably mantle the olivine confirming the origin of tholeiitic magma. Crystals of olivine surrounded by pyroxene or between spaces of plagioclase laths. Olivine in some cases altered into chlorite by fibrous of green color. Stages of alteration Progression of olivine are observed that entire alteration to minerals of brown color, it is likely that an iron oxides mixtures in many stages of hydration and oxidation, (Fig.10b) involved with chlorite **[37]. Magnetite** crystals is irregular and ranging in size from small to large grains scattered between pyroxene and olivine crystals (Figs.10a, b, c) (Figs.11a, b).

4.1.3.2 Quartz arenite:

This type of microfacies is recorded in lower part of Hagul Formation (samples no 2-3, 15-1). It is composed of pale yellow, medium to fine, semi hard and planner cross bedded sandstones intercalated with thin lenses of mudstone. At the Hagul Formation this sandstone type of facies overlies weathered basalt of Oligo-Miocene age.

Petrographically, this sandstone facies varies in sizes from medium to fine sand and the main size is (0.6 mm), moderately sorted, monocrystalline, sometime polycrystalline, sub-angular, elongated to spherical quartz grains occupying > 95% of the samples in an open packing texture (Fig.11c). Few (<5%) of rock fragments and feldspar grains can be determined in this type of facies (Fig.11d). The cement of the sandstone is made up of siliceous and calcareous.

4.2 Radiometric analysis:

Table 2 shows that the samples of soil and doleritic basaltic rocks at depths from 2 to 15 m, C_U ranges from 1.24 to 13.59 with an average 7.09, C_{Th} ranges from 8.12 to 20.3 with an average 15.41, C_{Ra} ranges from 22.2 to 55.5 with an average 39.56 and C_k range from 71.99 to 369.34 with an average 249.12, all

radiometric measurements for all samples are under the allowest permissible limit (370 Bq/Kg) recommendable by International Atomic Energy Agency **[38].** Also, the data of measured of Ra_{eq} in **Table (2**), for soil and doleritic basaltic rocks samples varied from 47.09 to 108.87 (Bq/kg) with an average is 80.78 (Bq/kg), which is much lower than the allowed limits 370 (Bq/kg) as recommendable by **[38].** The observed of highest and less values of annual effective dose is 62.94 (μSvy^{-1}) and 26.78 (μSvy^{-1}) respectively with a mean average value 46.79 $\mu Svyr^{-1}$, which is less than 70 $\mu Svyr^{-1}$ is the highest value permitted value **[39]**. The observed of highest and lowest values of the external hazard index is 0.29 and 0.13 (Bq/kg) respectively with a mean average (0.218).

All of radiometric analysis of the samples in the study area are lower than recommendable value by the **[38]** which confirms that the radiation risks indicators are included under the permissible limits and safety for human's activities and building in the study area.

5 CONCLUSION:

This article includes the sedimentological and radiometric studies of foundation beds of some localities of New Administrative Capital of Egypt. The sedimentary properties of subsurface sediments in the study area and the statistical grain size parameters reveal that, the subsurface sediments are generally sands. The graphic mean size values indicate the dominance of medium sand size, with very poorly sorted and strongly fine-skewed. According to this study, most of the studied samples are leptokurtic. Textural characteristics strongly suggest that river conditions were most probably the dominating factors controlling the transportation and accumulation of the investigated sands. X-ray diffraction analysis indicates that the clay minerals of the studied samples are montmorillonite and kaolinite. The dominant mineral in the studied clay samples is montmorillonite, whereas montmorillonite has danger and harmful effect on construction and buildings as a result of swelling character higher than any of clay minerals. Petrographically, the studied samples can be classified into basaltic rocks which are classified as doleritic basalt and non-carbonate microfacies which include quartz arenite type. Furthermore, the radiometric examination and results indicate that the studied localities of New Administrative Capital is more safe radiation for human activities.

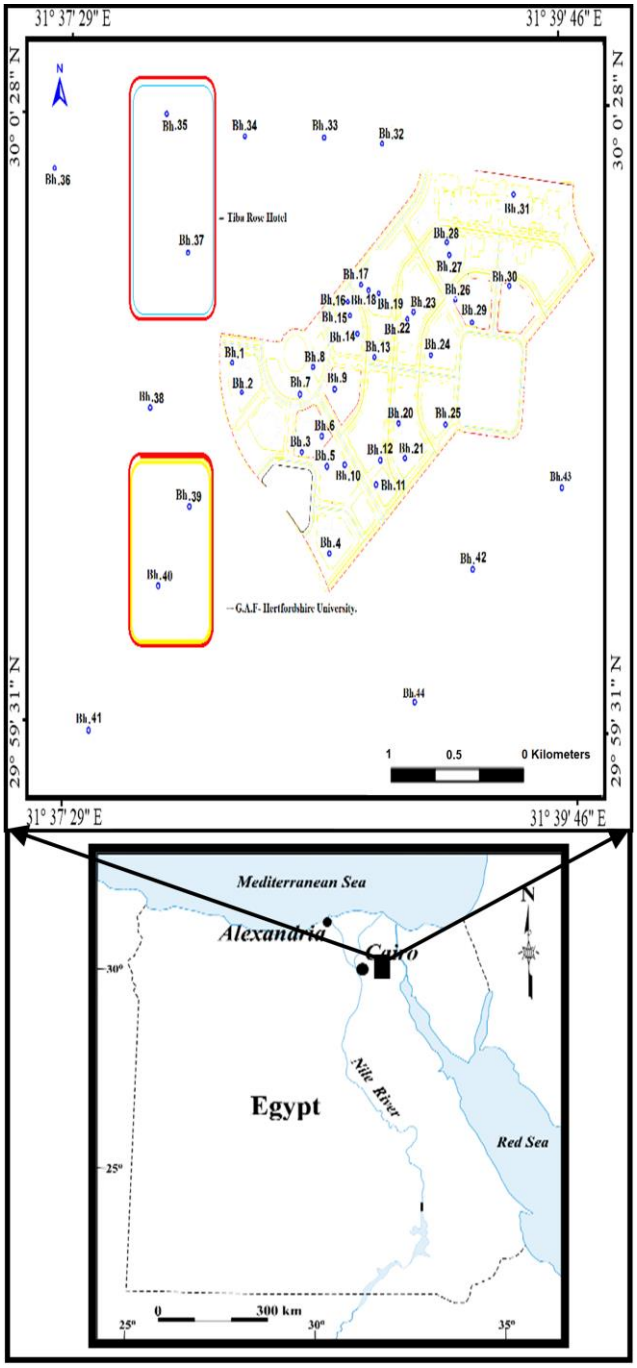

Fig. (1). Location map of the study area with boreholes and measured sections.

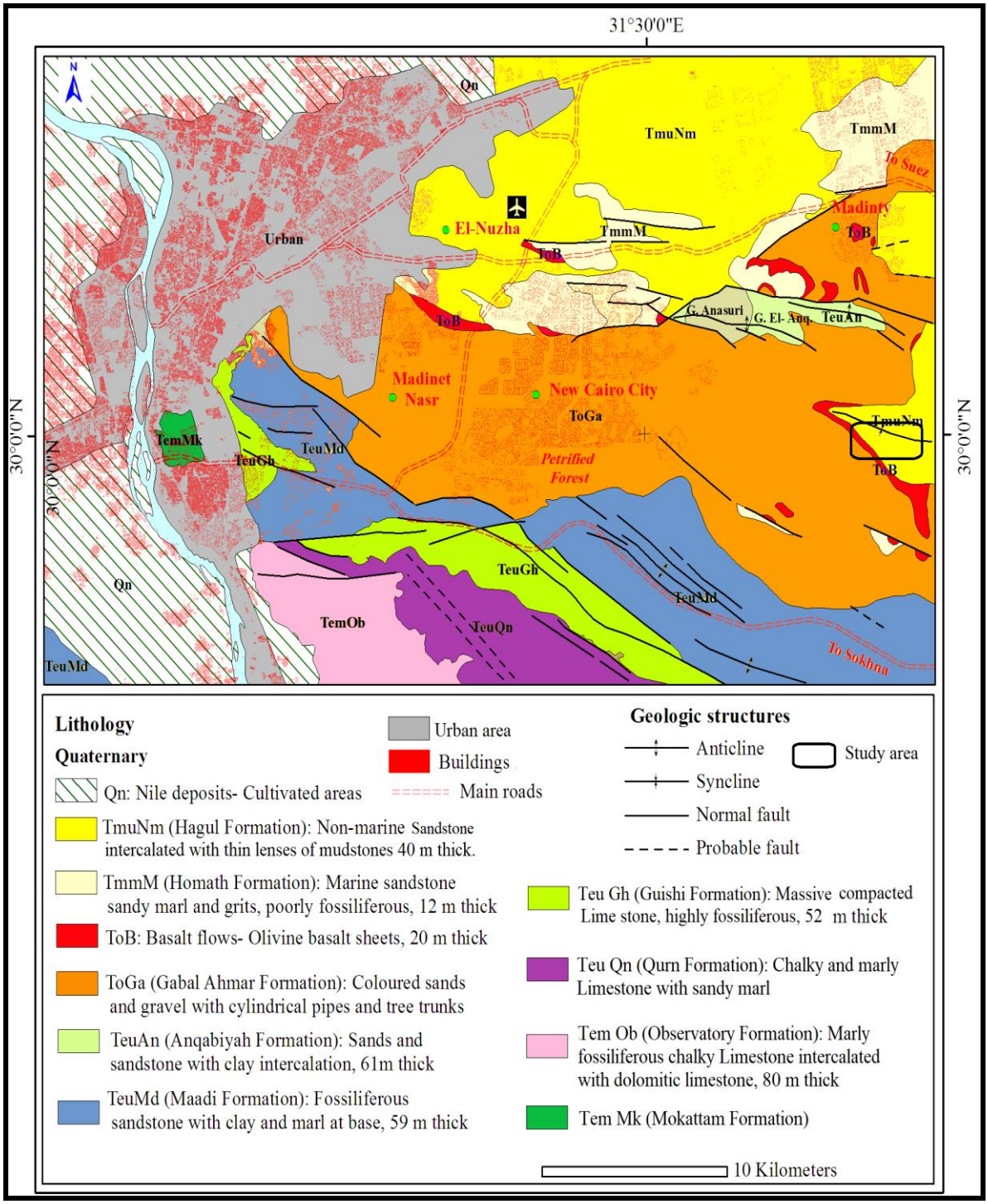

Fig. (2). Geological map of Cairo-Suez Disrict and location of study area (**Modified after Conoco, 1987**).

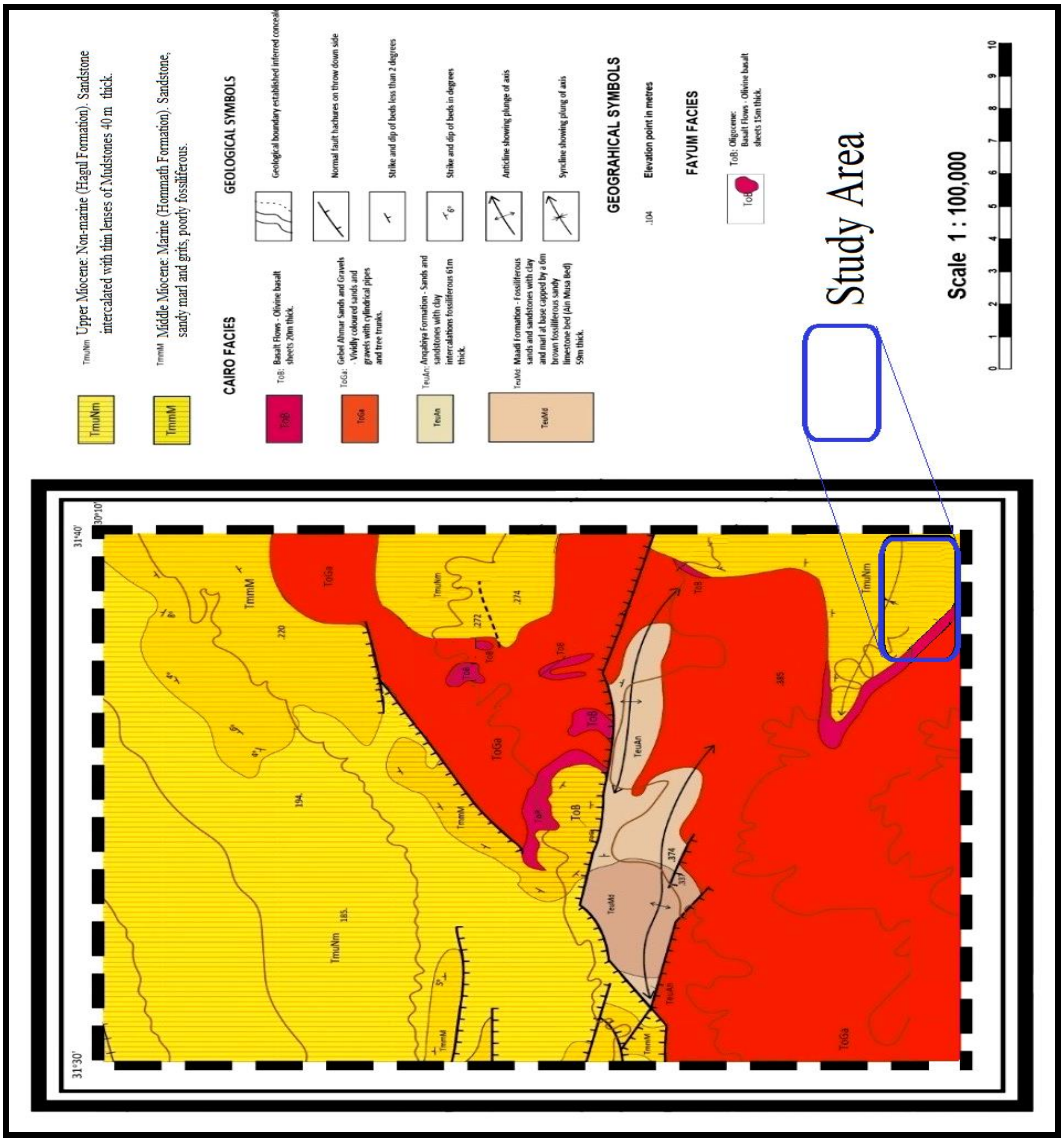

Fig. (3). Structure geologic map of the Study area **(EGSMA, 1983) [40].**

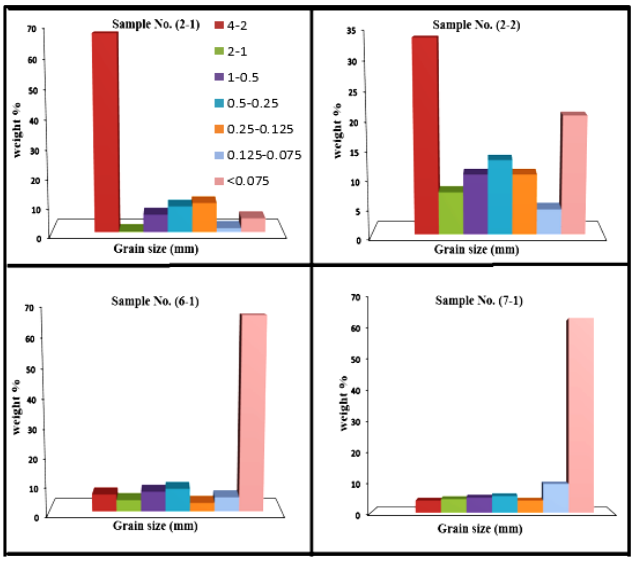

Fig. (4). Histograms of some studied samples

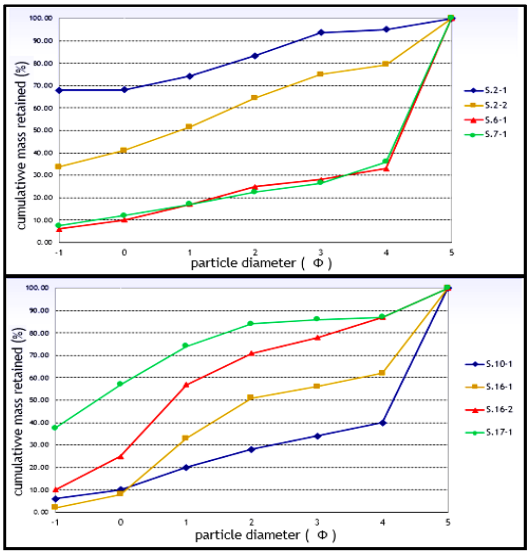

Fig. (5). Cumulative curves of the studied samples

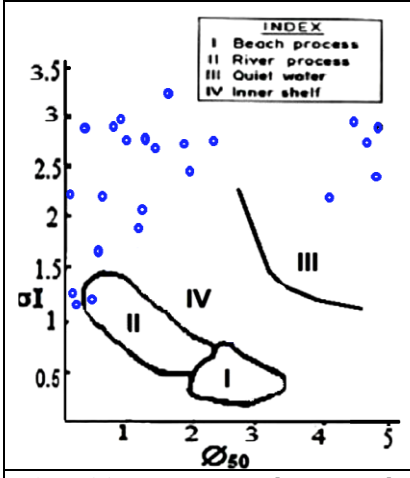

Fig. (6). Diagram showing the standard deviation (σI) versus median (Φ50) of the studied samples (after Stewart, 1958).

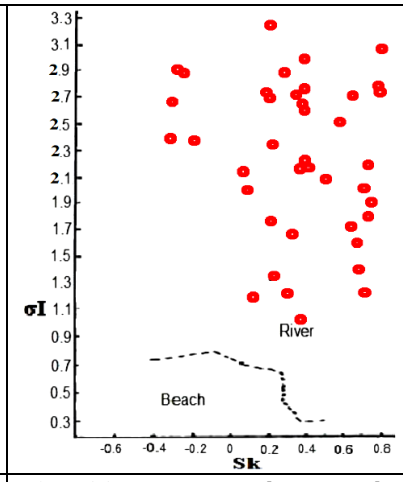

Fig. (7). Diagram showing the standard deviation (σI) versus skewness (SK) of studied samples (after Friedman, 1967).

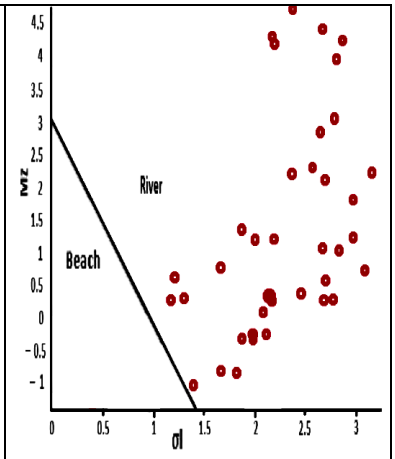

Fig. (8). Diagram showing the standard deviation (σI) versus mean size (Mz) of studied samples (after Moiola and Weiser, 1968).

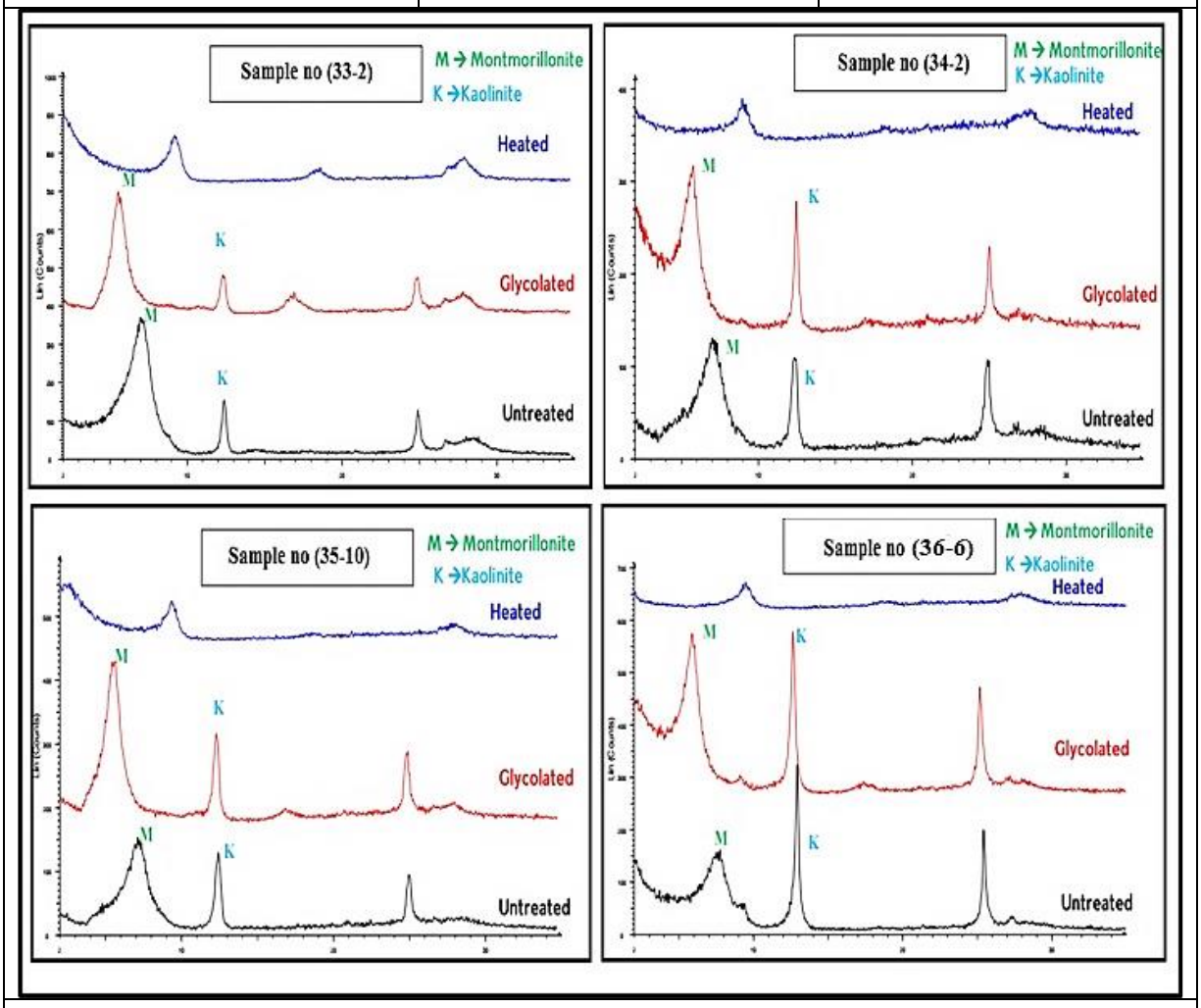

Fig. (9). X-ray diffraction of some studied clay samples, (samples 33-2, 34-2 35-10 and 36-6).

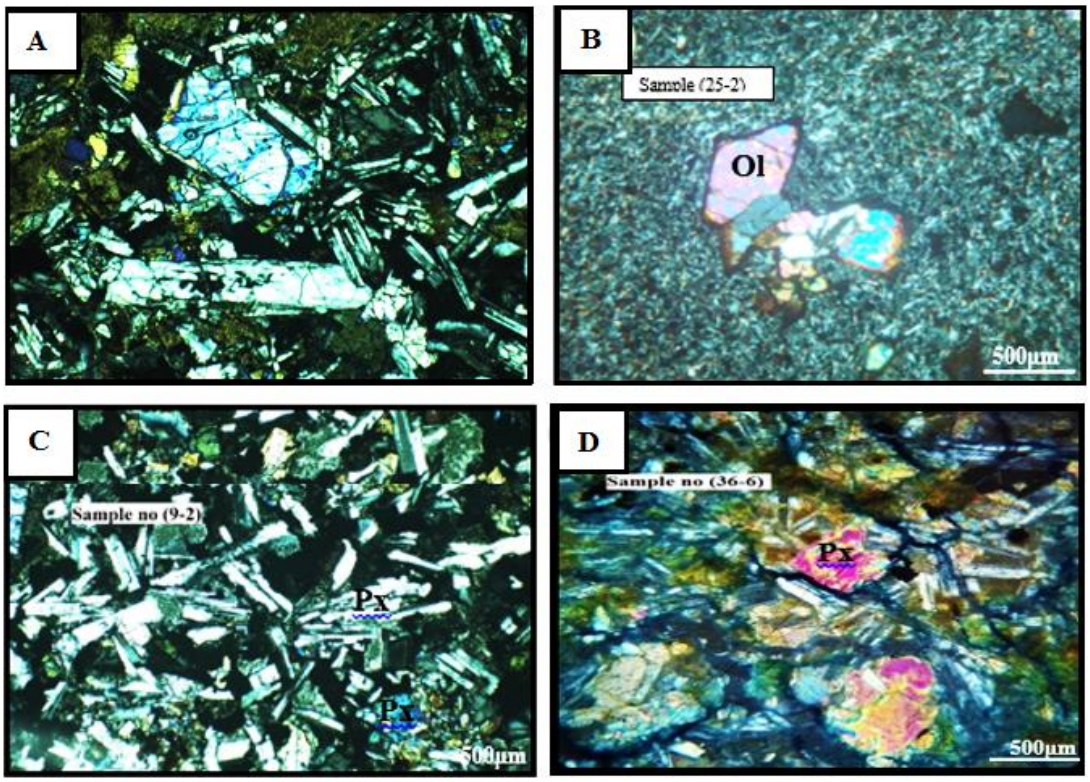

Fig. (10). Photomicrographs showing the weathered basalt samples at the study area. **(A)** Pyroxene (PX) forming ophitic and subophitic texture in doleritic basalt and alteration of pyroxene to chlorite. **(B)** Slightly altered olivine (Ol) large crystal in fine groundmass in the porphyritic doleritic basalt. **(C)** Plagioclase elongated crystals (Pl) with lamellar twinning in the doleritic basalt. **(D)** Pyroxene (PX) forming porphyritic texture in the porphyritic basalt.

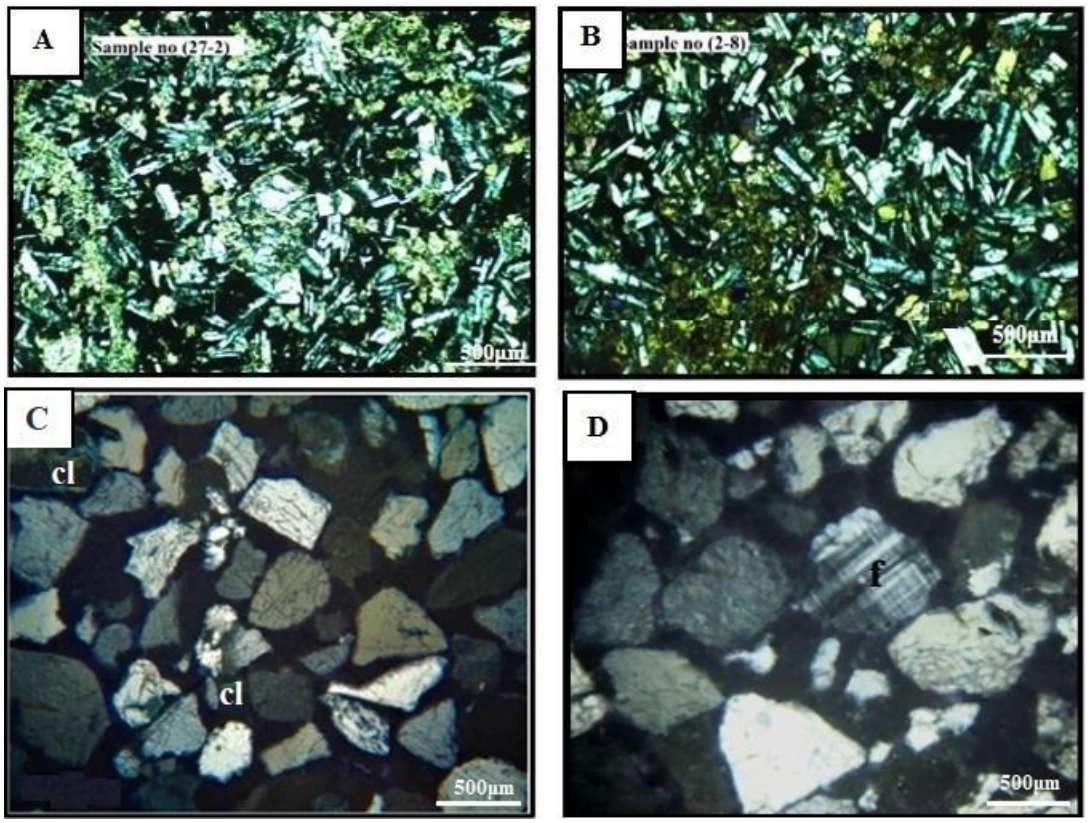

Fig. (11). Photomicrographs showing slightly altered doleritic basalt with Chlorite and iron oxides. **(A&B)** Quartz arenite facies type with traces of chlorite (cl) and feldspar (f) grains. **(C, D)**

Table 1: Grain size data of the studied samples.

Sample No.	Weight % of fraction							Median	Textural Parameters			
	4 – 2 (mm)	2 – 1 (mm)	1 - 0.5 (mm)	0.5 - 0.25 (mm)	0.25 - 0.125	0.125 - 0.075 (mm)	< 0.075 (mm)	Φ50	MZ	σI	SK	KG
2-1	67.9	0.2	6.2	9.1	10.3	1.4	4.9	-1.264	-0.323	1.806	0.751	0.849
2-2	33.6	7.4	10.5	13	10.5	4.4	20.6	0.857	1.341	2.889	0.31	0.849
6-1	6	4	7	8	3	5	67	4.819	4.219	2.872	-0.323	0.822
7-1	7.5	4.5	5	5.5	4	9.5	64	4.786	4.370	2.692	-0.271	1.053
10-1	6	4	10	8	6	6	60	4.447	3.97	2.901	-0.251	0.785
16-1	2	6	25	18	5	6	38	1.944	2.823	2.674	0.416	0.721
16-2	10	15	32	14	7	9	13	0.781	1.224	2.214	0.372	1.253
17-1	37.5	19.5	17	10	2	1	13	-0.359	0.023	2.14	0.477	1.386
18-1	4	7	23	8	15	4	39	2.533	3.001	2.768	0.208	0.731
20-1	64	14	8	6	1	1	6	-1.219	-0.740	1.59	0.677	1.871
22-1	58.5	13.5	9	5	2.5	1.5	10	-1.145	-0.424	2.011	0.726	1.674
23-1	21	5	17	11	6	2	38	1.636	2.201	3.255	0.244	0.699
24-1	18	9	23	16	4	3	27	1	1.788	3	0.375	0.856
31-1	4	12	25.5	15.5	7	9	27	1.548	2.341	2.6	0.414	0.9
35-1	91	0.7	1.3	1	1	0.5	4.5	0	0.358	2.230	0.391	1.065
35-2	92.1	3.6	9.3	13	9.6	3.8	18.6	0.462	1.058	2.812	0.382	0.866
36-1	6.9	26.1	30	20.5	6.5	1	9	0.567	0.664	1.729	0.287	1.496
36-2	0	19	22	29	17	1.8	11.2	1.310	1.325	1.781	0.208	1.386
36-3	35.6	14.4	15	14	8	2.5	10.5	0	0.358	2.23	0.391	1.065
39-1	72.6	3.3	7.7	4.4	3	0.7	8.3	-1.311	-0.667	1.833	0.753	2.182
39-2	85.5	1.2	2.8	1.3	1.6	3.6	4	-1.415	-1.415	1.028	0.404	3.836
40-1	10.2	34.4	35.4	9	5.3	1.1	4.6	0.153	0.255	1.323	0.234	1.428
40-2	5.7	39.3	30	15.8	4.5	0.7	4	0.167	0.333	1.191	0.29	1.102
40-3	34.8	5.2	10	18	14	0.9	17.1	1	1.157	2.692	0.211	0.933
40-4	99.8	0	0	0	0	0	0.2	-1.499	-1.499	0.307	0	0.738
40-5	59	9.1	9.4	6.4	3.1	1.2	11.8	-1.153	0.283	2.169	0.753	1.438
42-1	5.3	29.7	28	22	10.4	0	4.6	0.536	0.617	1.257	0.151	0.875
42-2	48.9	2.1	1.4	12.6	16	6.1	12.9	-0.476	0.404	2.508	0.590	0.821
42-3	47.3	5.7	7	3.3	16.7	2.9	17.1	-0.526	0.608	2.729	0.642	0.85
42-4	6.6	16.4	21	18	11	1	26	1.333	2.094	2.727	0.391	0.907
42-5	61.1	1.9	1.5	2.5	7	1.9	24.1	-1.182	0.750	3.096	0.838	0.744
43-1	8	14	19	24.2	18.8	1.9	14.1	1.372	1.314	2.049	0.126	1.364
43-2	82.3	1.7	3	4.1	2.3	0.5	6.1	-1.392	-1.066	1.428	0.686	4.348
43-3	67.6	3.4	5.7	7.5	6.8	1.2	7.8	-1.26	-0.350	2.024	0.773	1.264
43-4	61.2	3.1	5.7	7	4.7	0.9	17.4	-1.183	0.386	2.772	0.820	1.078
44-1	64.4	8.6	7.5	3.2	3.9	1.2	11.2	-1.224	-0.299	2.172	0.775	1.750
44-2	7.5	7.1	15.4	21.3	18.7	8.9	21.1	1.939	2.266	2.430	0.212	1.246
44-3	60.2	7.8	6.4	3.6	4	1.1	16.9	-1.169	0.353	2.736	0.815	1.289
44-4	5.4	0.6	1.5	2.5	10	11.3	68.7	4.897	4.835	2.430	-0.203	1.150
44-5	5.6	1.9	3.5	2.5	2.3	3	81.2	5.375	5.195	2.368	-0.299	1.381
44-6	0.6	1.5	2.9	12	19	9.1	54.9	4.117	4.264	2.212	0.074	0.745

Abbreviations: Mz=Mean size; SK= Inclusive graphic skewness; KG= Kurtosis; σI= Inclusive standard deviation

Table 2: Show **t**he distribution concentrations of natural radionuclide, ^{232}Th, ^{238}U, ^{226}Ra and ^{40}K and also include radium equivalent Ra_{eq}, dose rate D, effective dose rate D_{eff} and external hazard index H_{ex} of the studied samples at depths from 2 m to 15 m.

Sample Type	Sample no	^{238}U Concentration	^{232}Th Concentration	^{226}Ra Concentration	^{40}K Concentration	Ra_{eq} (Bq/Kg)	Absorbed dose, D (nGy/h)	Effective dose rate, D_{eff} (μSv/y)	External hazard index, H_{ex} (Bq/Kg)
		Bq/Kg	Bq/Kg	Bq/Kg	Bq/Kg				
Soil	2-2	9.88	16.24	33.3	350.56	83.52	39.98	49.03	0.23
	3-1	13.585	20.3	44.4	359.95	101.15	48.02	58.89	0.27
	6-1	8.645	16.24	33.3	363.08	84.48	40.50	49.67	0.23
	14-1	12.35	20.3	44.4	322.39	98.25	46.46	56.98	0.27
	20-1	11.115	16.24	44.4	341.17	93.89	44.71	54.83	0.25
	22-1	9.88	12.18	33.3	356.82	78.19	37.71	46.25	0.21
	26-1	7.41	16.24	44.4	369.34	96.06	45.88	56.26	0.26
	29-1	8.645	16.24	33.3	316.13	80.87	38.56	47.29	0.22
	31-1	11.115	12.18	44.4	278.57	83.27	39.59	48.55	0.22
	34-1	8.645	20.3	33.3	294.22	84.98	40.18	49.28	0.23
	2-6	13.585	20.3	44.4	338.04	99.46	47.11	57.78	0.27
	15-3	11.115	16.24	55.5	291.09	101.14	47.75	58.57	0.27
	18-2	12.35	20.3	44.4	306.74	97.05	45.81	56.19	0.26
	21-2	11.115	20.3	44.4	341.17	99.70	47.24	57.93	0.27
	32-1	9.88	16.24	44.4	212.84	84.01	39.40	48.32	0.23
	43-7	12.35	16.24	55.5	300.48	101.86	48.14	59.04	0.28
	42-5	11.115	20.3	55.5	297.35	107.42	50.54	61.99	0.29
	44-4	9.88	16.24	44.4	272.31	88.59	41.86	51.34	0.24
	36-6	13.585	20.3	44.4	353.69	100.66	47.76	58.57	0.27
	42-7	9.88	16.24	55.5	272.31	99.69	46.98	57.61	0.27
	43-8	12.35	20.3	44.4	341.17	99.70	47.24	57.93	0.27
	44-12	11.115	20.3	55.5	316.13	108.87	51.32	62.94	0.29
	Total	239.59	389.76	976.80	6995.55	2072.81	982.74	1205.23	5.60
	Average	10.89	17.72	44.40	317.98	94.22	44.67	54.78	0.25
Basaltic rocks	3-2	1.235	12.18	33.3	147.11	62.04	29.03	35.60	0.17
	5-2	2.47	16.24	33.3	184.67	70.74	33.11	40.61	0.19
	9-2	1.235	12.18	22.2	200.32	55.04	26.12	32.03	0.15
	30-1	2.47	12.18	22.2	97.03	47.09	21.84	26.78	0.13
	2-8	2.47	12.18	33.3	106.42	58.91	27.35	33.54	0.16
	10-2	3.705	16.24	33.3	181.54	70.50	32.98	40.45	0.19
	12-2	1.235	12.18	33.3	90.77	57.71	26.70	32.74	0.16
	23-2	3.705	12.18	22.2	209.71	55.77	26.50	32.50	0.15
	25-2	1.235	8.12	33.3	118.94	54.07	25.33	31.07	0.15
	27-2	2.47	16.24	33.3	225.36	73.88	34.80	42.68	0.20
	28-2	1.235	12.18	44.4	71.99	67.36	31.04	38.06	0.18
	30-2	3.705	8.12	33.3	169.02	57.93	27.41	33.61	0.16
	32-2	2.47	16.24	33.3	206.58	72.43	34.02	41.72	0.20
	35-9	1.235	12.18	44.4	143.98	72.90	34.02	41.72	0.20
	37-5	3.705	12.18	33.3	269.18	71.44	34.08	41.80	0.19
	40-7	1.235	12.18	44.4	134.59	72.18	33.63	41.24	0.20
	39-4	1.235	8.12	33.3	162.76	57.44	27.15	33.29	0.16
	Total	37.05	211.12	566.10	2719.97	1077.44	505.11	619.46	2.91
	Average	2.18	12.42	33.30	160.00	63.38	29.71	36.44	0.17
Total		**276.64**	**600.88**	**1542.90**	**9715.52**	**3150.25**	**1487.85**	**1824.70**	**8.51**
Average		**7.09**	**15.41**	**39.56**	**249.12**	**80.78**	**38.15**	**46.79**	**0.218**
World value		**< 370**					**< 55**	**< 70**	**≤1**

REFERENCES

[1] Das BM, Sobhan K. Principles of geotechnical engineering. Cengage learning, Stamford, USA. 2013.

[2] Klopp HW, Arriaga FJ, Likos WJ, Bleam WF. Atterberg limits and shrink/swell capacity of soil as indicators for sodium sensitivity within a gradient of soil exchangeable sodium percentage and salinity. Geo derma. 2019; 35(3):449-458. https://doi.org/10.1016/j.geoderma.2019.07.016

[3] Stell E, Guevara M, Vargas R. Soil swelling potential across Colorado: a digital soil mapping assessment. Landsc Urban Plan. 2019; 190:10. https://doi.org/10.1016/j.landurbplan.2019.103599

[4] Thomas A, Tripathi RK, Yadu LK. Alkali-activated GGBS and enzyme on the swelling properties of sulfate bearing soil. Geomech Eng. 2019; 19(1):21-28. https://doi.org/10.12989/gae.2019. 19.1.021

[5] Sharma AK, Sivapullaiah PV. Ground granulated blast furnace slag amended fly ash as an expansive soil stabilizer. Soils Found. 2016; 56(2):205–212. https://doi.org/10.1016/j.sandf.2016.02.004

[6] Hoy M, Rachan R, Horpibulsuk S, Arulrajah A, Mirzababaei M. Effect of wetting–drying cycles on compressive strength and microstructure of recycled asphalt pavement–Fly ash geopolymer. Constr Build Mater. 2017; 144:624–634

[7] Yoobanpot N, Jamsawang P, Horpibulsuk S. Strength behavior and microstructural characteristics of soft clay stabilized with cement kiln dust and fy ash residue. Appl Clay Sci. 2017; 141:146–156.

[8] Moayedi H, Aghel B, MaM A, Nguyen H, Safuan A, Rashid A. Applications of rice husk ash as green and sustainable biomass. J Cleaner Prod. 2019; 237: 117851. https://doi.org/10.1016/j.jclepro.2019.117851

[9] Molina-Gomez F, Caicedo B, da Fonseca AV. Physical modelling of soil liquefaction in a novel micro shaking table. Geomech Eng. 2019; 19(3):229–240. https://doi.org/10.12989/gae.2019.19.3.229

[10] Sonmezer YB. Energy-based evaluation of liquefaction potential of uniform sands. Geomech Eng. 2019a; 17(2):145–156. https://doi.org/10.12989/gae.2019.17.2.145

[11] Kumar S, Sahu AK, Naval S. Influence of jute fiber on CBR value of expansive soil. Civ Eng J. 2020; 6(6):1180–1194. https://doi.org/10.28991/cej-2020-03091466.

[12] Sakr MAH, Saad AM, Ali EO, Moayedi H. Geotechnical parameters modelling and the radiation safety of expansive clayey soil treated with waste marble powder: a case study at west Gulf of Suez, Egypt. Environ Earth Sci. 2021; 80(7):1-18 https://doi.org/10.1007/s12665-021-09573-y

[13] Hefny K. Final report of the first stage of groundwater study in Greater Cairo. Res- Inst. groundwater (RIGW), 1982; 190. (In Arabic).

[14] Moustafa AR, Abd Allah AM. Structural setting of the central part of the Cairo Suez District. Earth sci. 1991; 5: 133-145.

[15] Moustafa AR, EL-Nahhas F, Abd El-Tawab S. Engineering geology of Mokattem City and its vicinity, Eastern Greater Cairo, Egypt. Eng Geol. 1991; 31: 327-344.

[16] Swedan AH. A note on the geology of Greater Cairo area. Ann Geol Sur. Egypt. 1991; 17: 239- 251.

[17] El-Nahhas F, Ahmed A. Deformation and strength characteristics of rock formations in Mokattam area, Proc. Int. Colloquium on Structural Engineering, Ain Shams Univ., Egyptian Society of Engineers and Canadian Society of civil Eng. 1992; 2: 561-571.

[18] Saad AM. Identification of Shadow Facies at New Cairo City Through their Petrophysical Characteristics, Using Compiled Geophysical, Engineering and Sedimentological Researches. Ph.D. Thesis, Fac. Sci., Al-Azhar Univ. 2005; 224 p.

[19] Saad AM. Mechanical behavior and geoelectrical analysis of shallow foundation beds at industrial area, New Cairo – Egypt. Mid-East J Appl Sci. 2016; 6 (3): 430-441.

[20] Saad AM, Thabet HS, Khaled MA, Tharwat HA, Warshal R. Evaluation of the different foundation beds at Barwa area by using geophysical and geotechnical studies. Int J Inno Sci Eng Tech. 2016; 3 (5): 127-140.

[21] Saad AM, Wajih M, Attia TM. Characterization and evaluation of the foundation beds at Mivida area – New Cairo City. Al Azhar Bull. Sci. 2018; 29 (1): 1-14.

[22] Hagag W. Structural evolution and Cenozoic tectonostratigraphy of the Cairo-Suez district, North Eastern Desert of Egypt: fifield-structural data from Gebel Qattamiya-Gebel

Um Reheiat area. J African Earth Sci. 2016; 118: 174–191.

[23] Abu Al Ezz MS. Landforms of Egypt. The American Univ. Press in Cairo UAR. 1971; p. 1-249.

[24] Faris MI, Abass HL. The geology of shabraweet area, bull. Fac. Sci., Ain Shams University, 1961; 6: 37-61.

[25] Folk RL, Ward WC. Brazes River bar, a study in the significance of grain size parameters. J sed Petrol. 1957; 27: 3-27.

[26] Blott SJ, Pye K. GRADISTAT: a grain size distribution and statistics package for the analysis of unconsolidated sediments. Earth Surf Proc Land f. 2001; 26 (11): 1237-1248.

[27] Wentworth CK. A scale of grade and class terms for clastic sediments. The J Geol. 1922; 30 (5): 377-392

[28] Stewart HJ. Sedimentary reflections on depositional environments in San Migue Lagoon, Baja California, Mexico. AAPG Bull. 1958; 42(11): 2567-2618.

[29] Friedman GM. Distinction between dune, beach and river sands from their textural characteristics. J Sed Petrol. 1961; 31: 515-529.

[30] Friedman GM. Dynamic processes and statistical parameters compared for size frequency distribution of beach and river sands. J Sed Petrol. 1967; 37 (2): 327-354.

[31] Moiola RJ, Weiser D. Textural parameters and evaluation. J Sed Petrol. 1968; 28: 211-226.

[32] Beretka I, Mathew PI. Natural radioactivity of Australian building materials, waste and byproducts. Health Phys. 1985; 48:87–95.

[33] El-Daly TA, Hussein AS. Natural radioactivity levels in environmental samples in north western desert of Egypt. Proceedings of the 3rd Environmental Physics Conference, Aswan, Egypt 19-23 Feb. 2008; 79-88

[34] United Nations Scientific Committee on the Effects of Atomic Radiation UNSCEAR. Exposure from natural sources of radiation. Forty-second session of United Nations Scientific Committee on the Effect of Atomic Radiation, Vienna 12-28 May. 1993b

[35] UNSCEAR. Sources and Effects of Ionizing Radiation. United Nations Scientific Committee on the Effects of Atomic Radiation, United Nations, New York. 2000; 2:49-72.

[36] International Society for Rock Mechanics ISRM. The Complete ISRM Suggested Methods for Rock Characterization Testing and Monitoring: 1974-2006. In: Ulu say, Hudson (Eds.) Suggested Methods Prepared by the Commission Testing Methods, Int. Soc. Rock Mech. ISRM Turkish National Group, Turkey., 2007; p.628.

[37] Fawcett JJ. Alteration products of olivine and pyroxene in basalt lavas from the Isle of Mull. Mineralogical Magazine. 1965; 35(269): 55-68.

[38] International Atomic Energy Agency IAEG. Rock and Soil Description and Classification for Engineering Geological Mapping: Report by IAEG Commission on Engineering Geological Mapping. Bull Int Assoc Eng Geol. 1981; 24: 235-274.

[39] Veiga N, Sanches RM, Anjos K. Measurement of natural radioactivity in Brazilian beach sands. Radiation measurements. 2006; 41(2): 189-196.

[40] Egyptian Geological Survey and Mining Authority EGSMA. Geological map of Greater Cairo area, scale 1:1000.000. 1983.

تطبيقات علي الدراسات الرسوبية والإشعاعية لتقييم التربة تحت السطحية لبعض المناطق في العاصمة الإدارية ، القاهرة مصر.

ابراهيم عثمان [1] ، احمد م. سعد [2] ، اسامه دراز [3]

1. الوطنية المصرية للحفر والخدمات البترولية ، المقطم ، القاهرة ، مصر.
2. قسم الجيولوجيا ، كلية العلوم (بنين) ، جامعة الأزهر ، القاهرة ، مصر.
3. قسم الاستكشاف بهيئة المواد النووية ، القطامية ، القاهرة ، مصر.

الملخص

يتضمن هذا البحث الدراسات الرسوبية والإشعاعية علي بعض المناطق بالعاصمة الإدارية الجديدة، القاهرة، مصر. حيث تهدف الدراسة الي تقييم خواص طبقات التأسيس للأغراض الهندسية من خلال التعرف علي معاملات التدرج الحبيبي وبيئات الترسيب وخواص طبقات الطين وذلك لتأثيرها المباشر علي طبقات الأساس وأيضا دراسة اشعاعية المنطقة من خلال عدة معاملات هي مكافئ الراديوم ومعدل الجرعة الفعالة ومؤشر الخطر الخارجي لمعرفة مدى تأثير هذه الإشعاعات على الأنشطة البشرية. تحتوي الدراسات الرسوبية دراسة التحليل الحجمي للحبيبات ودراسة التركيب المعدني والدراسة البتروجرافية وذلك لتحديد القياسات الإحصائية ومعاملات التدرج الحبيبي اللازمة لوصف أنماط الترسيب للعينات الرسوبية بمنطقة الدراسة ، وتشتمل هذه المعاملات الإحصائية علي متوسط حجمي بمتوسط 1.205ϕ وهذا يشير أن الرمال ذات حجم متوسط الحبيبات، وفرز الحبيبات بمتوسط 2.297ϕ وهذا يعني أن الحبيبات فقيرة الفرز جدا ومعامل الالتواء بمتوسط 0.361ϕ مما يعني أن الحبيبات عالية الالتواء جدا ومعامل التفرطح بمتوسط 1.26ϕ مما يدل أن الحبيبات مدببة التفرطح وعند عمل العلاقات بين معاملات التحليل الحجمي المختلفة تبين أن بيئة الترسيب السائدة في منطقة الدراسة هي بيئة نهرية . وتبين من تحليل الحيود للأشعة السينية للعينات المدروسة أن المعادن الطينية هي المنتموريلونايت والكاولينيت. وقد أبدت الدراسة البتروجرافية التي أجريت علي 8 عينات وجود التربة الفتاتية متمثلة في الحجر الرملي و الطيني وتبين منها أن المادة اللاحمة في التربة الفتاتية هي السيليكا والكربونات ووجود بقايا من البازلت المتحلل وتبين منها وجود بعض التغيرات. وأظهرت الدراسة الإشعاعية نشاطية النويات المشعة للثوريوم واليورانيوم والبوتاسيوم و مكافئ الراديوم بمتوسطات 7.09 و15.41 و249.12 و80.78 بيكريل/كجم علي الترتيب بينما متوسطات معدل الجرعة الفعالة(D_{eff}) ومؤشر الخطر الخارجي(H_{ex}) يمثل 46.79 ميكروسيفر/سنة و0.218 بيكريل/كجم علي الترتيب وتعد هذه القيم أقل بكثير من القيم المسموح بها من قبل الوكالة الدولية للطاقة الذرية للأمان الإشعاعي ومن النتائج السابقة تبين أن منطقة الدراسة آمنة اشعاعيا.